

## Research Article

# Study of Corrosion in a Biomass Boiler

**C. Berlanga and J. A. Ruiz**

*Escuela Técnica Superior de Ingenieros Industriales y Telecomunicación, Universidad Pública de Navarra, Campus de Arrosadía, 31006 Pamplona, Spain*

Correspondence should be addressed to J. A. Ruiz; joseantonio.ruiz@unavarra.es

Received 26 October 2012; Revised 18 December 2012; Accepted 18 December 2012

Academic Editor: Ahmed A. Mohamed

Copyright © 2013 C. Berlanga and J. A. Ruiz. This is an open access article distributed under the Creative Commons Attribution License, which permits unrestricted use, distribution, and reproduction in any medium, provided the original work is properly cited.

Biomass plants, apart from producing energy, help to reduce CO<sub>2</sub>(g) emissions. One of the biggest problems for their development is superheater corrosion due to fuel corrosivity, especially of the straw. This limits both the temperature of the vapour and also the effectiveness of the plant. In order to know more about the reactions which happen inside the boiler of biomass, thermodynamic calculations using software (HSC Chemistry) have been carried out. Field tests have been carried out in the Sangüesa Biomass Plant in Navarra (Spain): determination of the types of oxides and the deposits formed on the superheaters tubes as well as a program to measure temperatures. Finally, the global results are discussed.

## 1. Introduction

Currently, much attention has been drawn towards the burning of biomass for power production. One of the main reasons for this is the concern regarding the global warming caused by carbon dioxide (CO<sub>2</sub>) emissions. Biomass that is produced at the rate it is consumed is considered CO<sub>2</sub> neutral because during growth it accumulates the same amount of CO<sub>2</sub>(g) by photosynthesis as it releases during combustion.

Biomass includes a large variety of different fuels with different chemical composition and combustion characteristics. Wheat straw contains large amounts of potassium and chlorine, which are very undesirable due to their high corrosion power, so straw combustion is associated with some corrosion problems which are not encountered in coal-fire plants. The burned wheat straw studied in this paper contains typically 1.0 wt% K, 0.4 wt% Cl, and 0.15 wt% S. Its sulphur content influences the corrosion mechanism.

During combustion, potassium chloride and SO<sub>2</sub>(g) are released in the flue gas and through the condensation and deposition processes they will result in the formation of superheater deposits rich in potassium chloride and potassium sulphate.

In actual power stations, it proved to be difficult to relate specific parameters to corrosion observation from test

superheaters, as so many of the parameters, such as temperature, ash deposit composition, and gas composition, were continually fluctuating.

There are many field and laboratory studies [1–16] which investigate the mechanics of corrosion due to straw burning, and some corrosion models based on chlorination have been suggested. Also, the use of chemical additives has been proposed to minimize this problem [17–21] in combination with mathematical models used to simulate the deposition behavior based on computational fluids dynamics [22].

To understand the corrosion mechanism of corrosion that superheaters tubes suffer it is necessary to know more about chemical reactions that happen in the boiler. To do so, a valid tool is the realization of thermodynamic calculations [23–25].

The focus of this work is the realization of thermodynamic calculations starting from the reactions that take place among the metals of the superheaters with the combustion atmosphere and the deposits that are formed on the tubes.

We have also carried out field tests. The Sangüesa Power Station belongs to Acciona Energia and is located in Navarra (Spain). It has a grate-fire boiler with a power of 25 MWth.

The most corrosive conditions in the plant happen in the third superheater which is in the third pass and has an outlet steam temperature of 540°C. The temperature of the metal is

calculated to be at 570°C. The gas temperature at this point was 850–900°C. The fuel used in the power station was only straw; straws studied will cause high temperature superheater corrosion when fired alone in power plants (with steam temperature higher than 420°C). Fly ash from straw firing on grate was rich in the volatile elements K, Cl, and S [4].

To complete the thermodynamic calculations, the deposits formed on the superheaters tubes as well as the oxides formed on the tubes have been characterized. The final objective of this work is to contribute to the knowledge of the corrosion that superheaters tubes suffer in the biomass plants and, in this way, contribute to the development of the biomass as industrial fuel for obtaining energy.

## 2. Experimental Procedures

**2.1. Thermodynamic Calculations.** The program “HSC Chemistry for Windows” [26] has been employed to calculate equilibrium compositions in several sets of systems related to hot corrosion reactions.

To calculate an equilibrium composition the HSC program redistributed the input elements among the various species such that the total Gibbs energy of the system was minimized, subject to the constraints that all interacting species were in equilibrium with each other and that the mass of the elements was conserved. Thermodynamically, this corresponded to a closed system calculation.

It is important to bear in mind the limitations of these calculations obtained with this program. As a simplification, activity coefficients were taken as 1.0. On the other hand, there is no presumption about whether the salt phase is liquid or solid. Obviously, the issue of whether a liquid salt phase exists at the given temperature is important to the kinetics of corrosion, but not to the calculation of an equilibrium composition.

Also the solubility in the solid state has not been considered. For example, placing Fe and Cr into the “metal” phase is computationally equivalent to assuming they are soluble and exist as a single phase.

The first step in the equilibrium calculation is the definition of the system. To do so, the calculations have been carried out on a small scale although the results are considered valid for bigger scales. The chemical composition of the alloy AISI 347 CG has been used to introduce the values of the metallic elements (Table 1).

The composition of the gasses has been based on the representative composition of the atmosphere of biomass combustion (Table 2).

The selected salt has been KCl(s) because it is the one found in the greatest quantities, closest to the surface of the tube. The quantity of salt introduced in the calculus has been the following one: KCl(s): 1 g/74,5 g =  $1,34 \times 10^{-5}$  k moles. The species obtained in the calculations were grouped into phases: gas, metal, oxide(s), and salts.

In the calculations, the effect of the variation of the temperature and of the quantity of HCl(g) and Cl<sub>2</sub>(g) on the different chemical compounds has been proved. These factors are considered the most influential in relation to the corrosion mechanism.

TABLE 1: k moles of metallic elements introduced in the thermodynamic calculations.

	Fe	Cr	Ni	Mn	Mo	Nb
AISI 347 CG	$5.2 \times 10^{-4}$	$1.3 \times 10^{-4}$	$7.5 \times 10^{-5}$	$5.2 \times 10^{-4}$	—	—

The first variable is the temperature; in this way the stable compounds are observed in the range of temperatures between 300°C and 900°C (with increments of 86°C) analyzing especially the temperature of 557°C. The second and third variables are the increments of HCl(g) and Cl<sub>2</sub>(g) (maintaining constant the temperature of 600°C) that are related, since both suppose a contribution of chlorine; the quantity of HCl(g) and Cl<sub>2</sub>(g) has been increased in 8 steps of the same magnitude ( $3.1 \times 10^{-8}$  k moles) until reaching a percentage in the gassy mixture of 4,7%; in this way, the effect of the possible variations of the composition of the biomass and in consequence of the combustion gasses has been proved.

**2.2. Deposits Characterization.** Deposits formed on the superheater were studied as composition can yield interesting information about the corrosion mechanism. Deposits were collected from the boiler superheaters during one plant stop.

Their chemical composition by scanning electron microscopy combined with energy dispersive X-ray analyses (SEM-EDX) and bulk chemical analyses (ICP-AES) was performed. The melting point of the inner layer was determined by differential scanning calorimetry (DSC).

**2.3. Oxides Characterization.** The structure of the oxides formed on the superheater tubes was determined by means of X-ray diffraction.

**2.4. Temperature Measurement.** Due to the influence of the temperature in the corrosion mechanism a program of the temperatures. Measurement was carried out. Type K of NiCr-Cr thermopars were used and they were protected with SiC powder.

## 3. Results and Discussion

### 3.1. Thermodynamic Calculations

**3.1.1. Influence of the Temperature (300°C–900°C).** The results of the thermodynamical calculations of the solid and gaseous species appear in Table 3 versus the influence of the temperature.

**Gaseous Species.** Three of the gaseous species introduced in the calculations (N<sub>2</sub>(g), CO<sub>2</sub>(g), and H<sub>2</sub>O(g)) are stable in the whole range of temperatures, while O<sub>2</sub>(g) and SO<sub>2</sub>(g) are consumed in different reactions with the rest of elements to form different compounds. The forming of metallic chlorides increases as the temperature increases. FeCl<sub>2</sub>(g) and CrCl<sub>2</sub>(g) present a quantity of  $7.0 \times 10^{-18}$  k moles and

TABLE 2: k moles of gaseous species introduced in the thermodynamic calculations.

	N <sub>2</sub> (g)	CO <sub>2</sub> (g)	O <sub>2</sub> (g)	HCl (g)	H <sub>2</sub> O (g)	SO <sub>2</sub> (g)	Cl <sub>2</sub> (g)
% weight	74.0	10.7	5.4	0.036-4.7	9.8	0.005	0.036-4.7
k moles	$3.3 \times 10^{-6}$	$4.8 \times 10^{-7}$	$2.4 \times 10^{-7}$	$1.6 \times 10^{-9}$ - $2.1 \times 10^{-7}$	$4.4 \times 10^{-7}$	$2.4 \times 10^{-10}$	$1.610^{-9}$ - $2.1 \times 10^{-7}$

TABLE 3: Results of the thermodynamical calculations of the solid and gaseous species as a function of temperature for the stainless steel AISI 347 CG.

Temperature (°C)	300	386	471	557	643	729	814	900
Gases								
N <sub>2</sub> (g)	3.3E-06	3.3E-06	3.3E-06	3.3E-06	3.3E-06	3.3E-06	3.3E-06	3.3E-06
CO <sub>2</sub> (g)	4.8E-07	4.8E-07	4.8E-07	4.8E-07	4.8E-07	4.8E-07	4.8E-07	4.8E-07
O <sub>2</sub> (g)	1.0E-36	1.0E-36	1.0E-36	1.0E-36	1.0E-36	2.2E-35	2.6E-32	1.1E-29
HCl (g)	3.1E-09	4.3E-09	4.9E-09	7.0E-09	1.4E-08	2.9E-08	5.4E-08	8.7E-08
SO <sub>2</sub> (g)	1.2E-31	1.3E-31	1.3E-31	1.3E-31	1.3E-31	1.3E-31	1.3E-31	1.3E-31
Cl <sub>2</sub> (g)	1.0E-36	8.6E-35	8.7E-32	3.5E-29	9.9E-27	1.5E-24	1.1E-22	3.6E-21
CrCl <sub>2</sub> (g)	4.2E-25	1.2E-22	7.3E-21	3.1E-19	1.4E-17	4.6E-16	8.8E-15	9.9E-14
CrCl <sub>3</sub> (g)	3.6E-26	5.0E-24	1.5E-22	4.5E-21	2.4E-19	1.1E-17	2.6E-16	3.5E-15
CrO <sub>2</sub> Cl (g)	1.0E-36	1.0E-36	1.0E-36	9.1E-36	3.7E-32	4.3E-29	1.6E-26	2.4E-24
CrO <sub>2</sub> Cl <sub>2</sub> (g)	1.0E-36	1.0E-36	1.0E-36	1.0E-36	1.0E-36	6.5E-34	4.0E-31	8.7E-29
CrO <sub>3</sub> (g)	1.0E-36	1.0E-36	1.0E-36	1.0E-36	1.0E-36	1.0E-36	4.8E-34	2.9E-31
FeCl <sub>2</sub> (g)	2.0E-23	4.4E-21	2.0E-19	7.0E-18	2.7E-16	7.6E-15	1.2E-13	1.2E-12
FeCl <sub>3</sub> (g)	1.9E-33	2.4E-30	3.9E-28	4.6E-26	7.0E-24	7.5E-22	3.8E-20	9.2E-19
NiCl <sub>2</sub> (g)	5.9E-31	8.7E-28	1.8E-25	2.0E-23	2.0E-21	1.3E-19	4.3E-18	7.9E-17
NiCl <sub>3</sub> (g)	1.0E-36	1.0E-36	1.0E-36	1.8E-35	1.6E-32	7.7E-30	1.4E-27	1.0E-25
H <sub>2</sub> O (g)	4.4E-07	4.4E-07	4.4E-07	4.4E-07	4.3E-07	4.3E-07	4.1E-07	4.0E-07
Metals								
Fe	5.2E-04	5.2E-04	5.2E-04	5.2E-04	5.2E-04	5.2E-04	5.2E-04	5.2E-04
Cr	1.3E-04	1.3E-04	1.3E-04	1.3E-04	1.3E-04	1.3E-04	1.3E-04	1.3E-04
Ni	7.5E-05	7.5E-05	7.5E-05	7.5E-05	7.5E-05	7.5E-05	7.5E-05	7.5E-05
Salts								
KCl	1.3E-05	1.3E-05	1.3E-05	1.3E-05	1.3E-05	1.3E-05	1.3E-05	1.3E-05
CrCl <sub>2</sub>	8.6E-10	2.4E-10	6.8E-11	4.3E-11	6.8E-11	1.4E-10	2.7E-10	5.9E-10
CrCl <sub>3</sub>	1.1E-15	2.9E-16	7.0E-17	4.9E-17	1.2E-16	4.6E-16	1.4E-15	5.0E-15
FeCl <sub>2</sub>	3.7E-12	4.5E-14	3.9E-14	6.0E-14	1.9E-13	9.0E-13	4.0E-12	1.4E-11
NiCl <sub>2</sub>	1.2E-12	3.8E-12	6.7E-12	1.81E-11	9.00E-11	4.86E-10	2.0E-09	6.4E-09
NiS	2.4E-10	2.4E-10	2.4E-10	2.4E-10	2.4E-10	2.4E-10	2.4E-10	2.4E-10
FeCl <sub>3</sub>	9.5E-30	8.4E-28	2.0E-26	5.5E-25	2.8E-23	1.2E-21	3.1E-20	4.2E-19
Oxides								
FeOCl	2.0E-22	1.1E-20	2.0E-19	2.6E-18	3.2E-17	3.0E-16	2.0E-15	9.7E-15
Cr <sub>2</sub> FeO <sub>4</sub>	3.6E-11	1.4E-10	4.1E-10	9.3E-10	1.8E-09	2.8E-09	3.9E-09	4.8E-09
Cr <sub>2</sub> O <sub>3</sub>	1.6E-07	1.6E-07	1.6E-07	1.6E-07	1.5E-07	1.4E-07	1.3E-07	1.1E-07
FeO	2.9E-16	6.0E-15	6.3E-14	4.0E-13	1.8E-12	5.7E-12	1.5E-11	3.0E-11
Fe <sub>2</sub> O <sub>3</sub>	8.0E-35	4.1E-31	2.9E-28	5.5E-26	3.8E-24	1.3E-22	2.2E-21	2.4E-20
Fe <sub>3</sub> O <sub>4</sub>	1.0E-36	3.4E-36	1.5E-32	1.3E-29	3.2E-27	3.0E-25	1.2E-23	2.8E-22
KCrO <sub>2</sub>	3.1E-15	1.4E-13	3.1E-12	2.8E-11	1.1E-10	2.8E-10	5.1E-10	7.5E-10
KFeO <sub>2</sub>	3.5E-32	3.0E-28	3.6E-25	7.8E-23	4.1E-21	8.6E-20	9.4E-19	6.3E-18
NiO	8.3E-21	3.7E-19	6.7E-18	6.7E-17	4.3E-16	1.9E-15	6.5E-15	1.7E-14

$3.1 \times 10^{-19}$  k moles, respectively, at  $557^\circ\text{C}$  while the formation of  $\text{NiCl}_2(\text{g})$  is very low ( $7.9 \times 10^{-19}$  k moles).

Finally, it should be noted that while  $\text{Cl}_2(\text{g})$  wastes react completely in the different reactions, the quantity of  $\text{HCl}(\text{g})$  is increased with the increasing temperature.

**Solids Species.** The metallic chlorides are formed in low quantities; at  $557^\circ\text{C}$   $\text{CrCl}_2(\text{s})$  presents  $4.3 \times 10^{-11}$  k moles,  $\text{FeCl}_2(\text{s})$   $6.0 \times 10^{-14}$  k moles, and only a negligible quantity of  $\text{NiCl}_2(\text{s})$  is formed. Among the metallic oxides,  $\text{Cr}_2\text{O}_3(\text{s})$  is the most stable with a great difference with respect to the test. At  $557^\circ\text{C}$ ,  $1.6 \times 10^{-7}$  k moles are formed and it stays constant in the whole range of temperatures. The  $\text{FeO}(\text{s})$  is the oxide of more stable iron presenting  $4.0 \times 10^{-13}$  k moles at  $557^\circ\text{C}$ , and their formation is favored with the temperature ( $3.0 \times 10^{-11}$  k moles to  $900^\circ\text{C}$ ).  $\text{NiO}(\text{s})$  is formed in a very small quantity of  $6.7 \times 10^{-17}$  k moles. Finally,  $\text{Cr}_2\text{FeO}_4(\text{s})$  is an oxide that it is formed in a considerable quantity of  $9.3 \times 10^{-10}$  k moles.

The quantity of metallic elements remains constant in the whole range of temperatures. The preference of the nickel to form  $\text{NiS}(\text{s})$  is worth highlighting, since it forms  $8.2 \times 10^{-10}$  k moles. The quantity of  $\text{KCl}(\text{s})$  remains constant in the whole range of temperatures.

**3.1.2. Influence of the Quantity of  $\text{HCl}(\text{g})$  ( $5.0 \times 10^{-9}$ – $1.8 \times 10^{-7}$  k moles) ( $T = 600^\circ\text{C}$ ).** The results of the thermodynamical calculations of the solid and gaseous species appear in Table 4 versus the influence of the quantity of  $\text{HCl}(\text{g})$ .

**Gaseous Species.** Three of the gaseous species of departure ( $\text{N}_2(\text{g})$ ,  $\text{CO}_2(\text{g})$ , and  $\text{H}_2\text{O}(\text{g})$ ) are stable. Metallic chlorides are present in low quantities, but their formation is favored with the increment of  $\text{HCl}(\text{g})$ .  $\text{FeCl}_2(\text{g})$  and  $\text{CrCl}_2(\text{g})$  present a quantity of  $1.5 \times 10^{-14}$  k moles and  $7.1 \times 10^{-16}$  k moles, respectively. Finally, it should be noted that while  $\text{Cl}_2(\text{g})$  is consumed almost in its entirety in the different reactions, the quantity of  $\text{HCl}(\text{g})$  remains constant.

**Solids Species.** The metallic chlorides are present in low quantities, but their formation is favored with the increment of  $\text{HCl}(\text{g})$ ;  $\text{CrCl}_2(\text{s})$  presents a maximum quantity of  $1.6 \times 10^{-8}$  k moles,  $\text{FeCl}_2(\text{s})$   $3.3 \times 10^{-11}$  k moles, and  $\text{NiCl}_2(\text{s})$   $1.6 \times 10^{-15}$  k moles. The formation of metallic oxides is not affected by the variation of  $\text{HCl}(\text{g})$ ;  $\text{Cr}_2\text{O}_3(\text{s})$  is the most present with  $1.6 \times 10^{-7}$  k moles; the  $\text{FeO}(\text{s})$  is the most stable iron oxide of more stable iron with  $8.8 \times 10^{-13}$  k moles and  $\text{NiO}(\text{s})$  is formed in a minimum quantity of  $1.8 \times 10^{-16}$  k moles. Finally,  $\text{Cr}_2\text{FeO}_4(\text{s})$  is a mixed oxide with an appreciable quantity of  $1.3 \times 10^{-9}$  k moles. The quantity of metallic elements remains constant in the whole range of concentration of  $\text{HCl}(\text{g})$ . The preference of the nickel to form  $\text{NiS}(\text{s})$  is worth highlighting since it forms  $8.2 \times 10^{-10}$  k moles. The quantity of  $\text{KCl}(\text{s})$  remains constant in the whole range of temperatures.

**3.1.3. Influences of the Quantity of  $\text{Cl}_2(\text{g})$  ( $5 \times 10^{-9}$ – $1.8 \times 10^{-7}$  k moles) ( $T = 600^\circ\text{C}$ ).** **Gaseous Species.** Three of the gaseous species introduced in the calculations ( $\text{N}_2(\text{g})$ ,  $\text{CO}_2(\text{g})$ , and  $\text{H}_2\text{O}(\text{g})$ ) are stable in the whole range of temperatures,

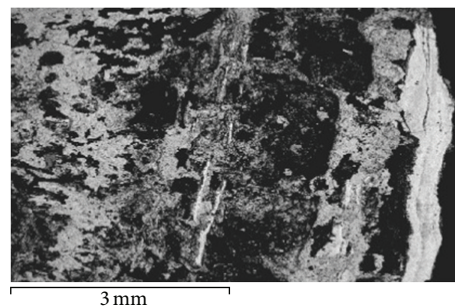


FIGURE 1: Inner and intermediate parts of the deposit. SEM Image ( $\times 20$ ).

while  $\text{O}_2(\text{g})$  and  $\text{SO}_2(\text{g})$  react completely with the rest of the elements, to form different compounds. The formation of metallic chlorides increases with the increment of  $\text{Cl}_2(\text{g})$ .  $\text{FeCl}_2(\text{g})$  and  $\text{CrCl}_2(\text{g})$  present a maximum quantity of  $1.5 \times 10^{-14}$  k moles and  $7.1 \times 10^{-16}$  k moles, respectively. The formation of  $\text{NiCl}_2(\text{g})$  is negligible. Finally, it should be noted that while  $\text{Cl}_2(\text{g})$  is consumed almost in its entirety in the different reactions, the quantity of  $\text{HCl}(\text{g})$  is increased with the concentration of  $\text{Cl}_2(\text{g})$ .

**Solids Species.** The metallic chlorides are present in low quantities, but their formation is favored with the increment of  $\text{Cl}_2(\text{g})$ ;  $\text{CrCl}_2(\text{s})$  presents  $1.6 \times 10^{-8}$  k moles,  $\text{FeCl}_2(\text{s})$   $3.3 \times 10^{-11}$  k moles, and  $\text{NiCl}_2(\text{s})$   $1.6 \times 10^{-15}$  k moles.

The formation of metallic oxides is not affected by the variation of  $\text{Cl}_2(\text{g})$ ;  $\text{Cr}_2\text{O}_3(\text{s})$  is the most present with  $1.6 \times 10^{-7}$  k moles while the  $\text{FeO}(\text{s})$  is most stable iron oxide of more stable iron presenting  $8.8 \times 10^{-13}$  k moles.  $\text{NiO}(\text{s})$  is formed in a minimum quantity of  $1.8 \times 10^{-16}$  k moles. Finally,  $\text{Cr}_2\text{FeO}_4$  is a mixed oxide with an appreciable quantity of  $13.10^{-9}$  k moles. The quantity of metallic elements remains constant in the whole range of temperatures. The preference of the neither to form  $\text{NiS}(\text{s})$  is worth noting since it forms  $8.2 \times 10^{-10}$  k moles. The quantity of  $\text{KCl}(\text{s})$  remains constant in the whole range of temperatures.

**3.2. Deposits Characterization.** In the figures one can observe the appearance of the deposits after 15000 h of operation. The superheaters tubes were completely covered by a 2–12 cm-thick layer of dark brown deposit. The deposit contained three distinct main layers: a thin dark brown outer layer, a thick white porous intermediate layer, and a complex inner thin layer (Figures 1 and 2). These three layers were studied separately (Table 5).

From the above data the three layers can be characterized as follows. The inner layer contains mainly potassium chloride (Figure 3(a)). There is a sublayer of iron oxides which come from the protective iron oxide scale of the superheater. There is no potassium sulphate. If sulphur is present in the deposit, it may react with potassium chloride, releasing chlorine [6].

In the inner layer, although potassium chloride is the principal component, we also find some potassium sulphate (Figure 3(b)). Fe-rich layers were observed indicating spallation of the iron oxide scale. At the outer part of this layer,

TABLE 4: Results of the thermodynamical calculations of the solid and gaseous species depending on quantity (k moles) of HCl (g) for the stainless steel AISI 347 CG.

HCl (g) (K moles)	4.9E-09	3.4E-08	6.1E-08	8.7E-08	1.1E-07	1.4E-07	1.6E-07	1.8E-07
Gases								
N <sub>2</sub> (g)	3.3E-06	3.3E-06	3.3E-06	3.3E-06	3.3E-06	3.3E-06	3.3E-06	3.3E-06
CO <sub>2</sub> (g)	4.8E-07	4.8E-07	4.8E-07	4.8E-07	4.8E-07	4.8E-07	4.8E-07	4.8E-07
O <sub>2</sub> (g)	1.0E-36	1.0E-36	1.0E-36	1.0E-36	1.0E-36	1.0E-36	1.0E-36	1.0E-36
HCl (g)	4.9E-09	3.4E-08	6.1E-08	8.7E-08	1.1E-07	1.4E-07	1.6E-07	1.8E-07
SO <sub>2</sub> (g)	1.2E-31	1.3E-31	1.3E-31	1.3E-31	1.3E-31	1.3E-31	1.3E-31	1.3E-31
Cl <sub>2</sub> (g)	1.6E-28	7.5E-27	2.4E-26	5.0E-26	8.2E-26	1.2E-25	1.6E-25	2.1E-25
CrCl <sub>2</sub> (g)	5.4E-19	2.5E-17	8.3E-17	1.7E-16	2.8E-16	4.0E-16	5.5E-16	7.1E-16
CrCl <sub>3</sub> (g)	4.1E-21	1.3E-18	7.8E-18	2.2E-17	4.7E-17	8.4E-17	1.3E-16	1.9E-16
CrO <sub>2</sub> Cl (g)	3.5E-34	2.4E-33	4.4E-33	6.2E-33	8.0E-33	9.7E-33	1.1E-32	1.3E-32
CrO <sub>2</sub> Cl <sub>2</sub> (g)	1.0E-36	1.0E-36	1.0E-36	1.0E-36	1.0E-36	1.0E-36	1.2E-36	1.5E-36
CrO <sub>3</sub> (g)	1.0E-36	1.0E-36	1.0E-36	1.0E-36	1.0E-36	1.0E-36	1.0E-36	1.0E-36
FeCl <sub>2</sub> (g)	1.1E-17	5.2E-16	1.7E-15	3.5E-15	5.7E-15	8.4E-15	1.1E-14	1.5E-14
FeCl <sub>3</sub> (g)	7.4E-26	2.4E-23	1.4E-22	4.0E-22	8.5E-22	1.5E-21	2.4E-21	3.5E-21
NiCl <sub>2</sub> (g)	5.3E-23	2.5E-21	8.1E-21	1.6E-20	2.7E-20	4.0E-20	5.4E-20	7.0E-20
NiCl <sub>3</sub> (g)	7.3E-35	2.4E-32	1.4E-31	4.0E-31	8.4E-31	1.5E-30	2.4E-30	3.5E-30
H <sub>2</sub> O (g)	4.4E-07	4.4E-07	4.4E-07	4.4E-07	4.4E-07	4.5E-07	4.5E-07	4.5E-07
Metals								
Fe	5.2E-04	5.2E-04	5.2E-04	5.2E-04	5.2E-04	5.2E-04	5.2E-04	5.2E-04
Cr	1.3E-04	1.3E-04	1.3E-04	1.3E-04	1.3E-04	1.3E-04	1.3E-04	1.3E-04
Ni	7.5E-05	7.5E-05	7.5E-05	7.5E-05	7.5E-05	7.5E-05	7.5E-05	7.5E-05
Salts								
KCl	1.3E-05	1.3E-05	1.3E-05	1.3E-05	1.3E-05	1.3E-05	1.3E-05	1.3E-05
CrCl <sub>2</sub>	1.3E-11	6.0E-10	2.0E-09	3.9E-09	6.5E-09	9.4E-09	1.3E-08	1.6E-08
CrCl <sub>3</sub>	9.1E-18	2.9E-15	1.7E-14	4.9E-14	1.0E-13	1.8E-13	2.8E-13	4.1E-13
NiS	2.4E-10	2.4E-10	2.4E-10	2.4E-10	2.4E-10	2.4E-10	2.4E-10	2.4E-10
NiCl <sub>2</sub>	1.3E-18	6.0E-17	2.0E-16	3.9E-16	6.4E-16	9.4E-16	1.3E-15	1.6E-15
FeCl <sub>2</sub>	2.6E-14	1.2E-12	3.9E-12	7.9E-12	1.3E-11	1.9E-11	2.5E-11	3.3E-11
NiS	2.4E-10	2.4E-10	2.4E-10	2.4E-10	2.4E-10	2.4E-10	2.4E-10	2.4E-10
FeCl <sub>3</sub>	4.9E-25	1.6E-22	9.2E-22	2.6E-21	5.5E-21	9.8E-21	1.5E-20	2.2E-20
Oxides								
FeOCl	4.7E-18	3.2E-17	5.8E-17	8.2E-17	1.1E-16	1.3E-16	1.5E-16	1.7E-16
Cr <sub>2</sub> FeO <sub>4</sub>	1.3E-09	1.3E-09	1.3E-09	1.3E-09	1.3E-09	1.3E-09	1.3E-09	1.3E-09
Cr <sub>2</sub> O <sub>3</sub>	1.6E-07	1.6E-07	1.6E-07	1.6E-07	1.6E-07	1.6E-07	1.5E-07	1.5E-07
FeO	8.9E-13	8.8E-13	8.8E-13	8.8E-13	8.7E-13	8.7E-13	8.6E-13	8.6E-13
Fe <sub>2</sub> O <sub>3</sub>	5.1E-25	5.1E-25	5.1E-25	5.1E-25	5.1E-25	5.0E-25	5.0E-25	5.0E-25
Fe <sub>3</sub> O <sub>4</sub>	2.4E-28	2.4E-28	2.3E-28	2.3E-28	2.3E-28	2.3E-28	2.3E-28	2.3E-28
KCrO <sub>2</sub>	1.2E-10	1.7E-11	9.7E-12	6.8E-12	5.3E-12	4.3E-12	3.7E-12	3.2E-12
KFeO <sub>2</sub>	1.3E-21	1.9E-22	1.1E-22	7.4E-23	5.7E-23	4.7E-23	4.0E-23	3.5E-23
NiO	1.8E-16	1.8E-16	1.8E-16	1.8E-16	1.8E-16	1.8E-16	1.7E-16	1.7E-16

TABLE 5: Chemical composition of deposits.

	Cl	K	S	Fe	Si	Ca	Mg	Na	Al	P
Inner deposit	32.7	35.4	0.2	5.2	1.2	0.1	<0.01	<0.01	<0.01	<0.01
Intermediate deposit	25.7	22.8	0.8	4.8	8.6	2.1	0.2	0.5	0.2	0.3
Outer deposit	12.5	14.2	1.9	2.2	18.5	3.3	0.8	0.9	0.5	0.5

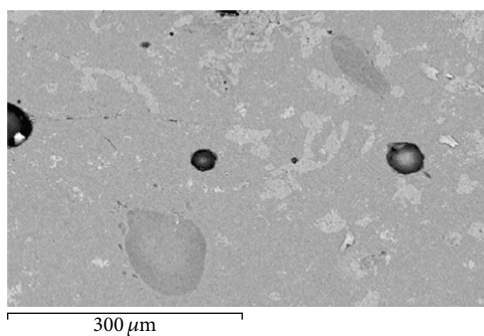


FIGURE 2: Outer part of the deposit SEM Image ( $\times 420$ ).

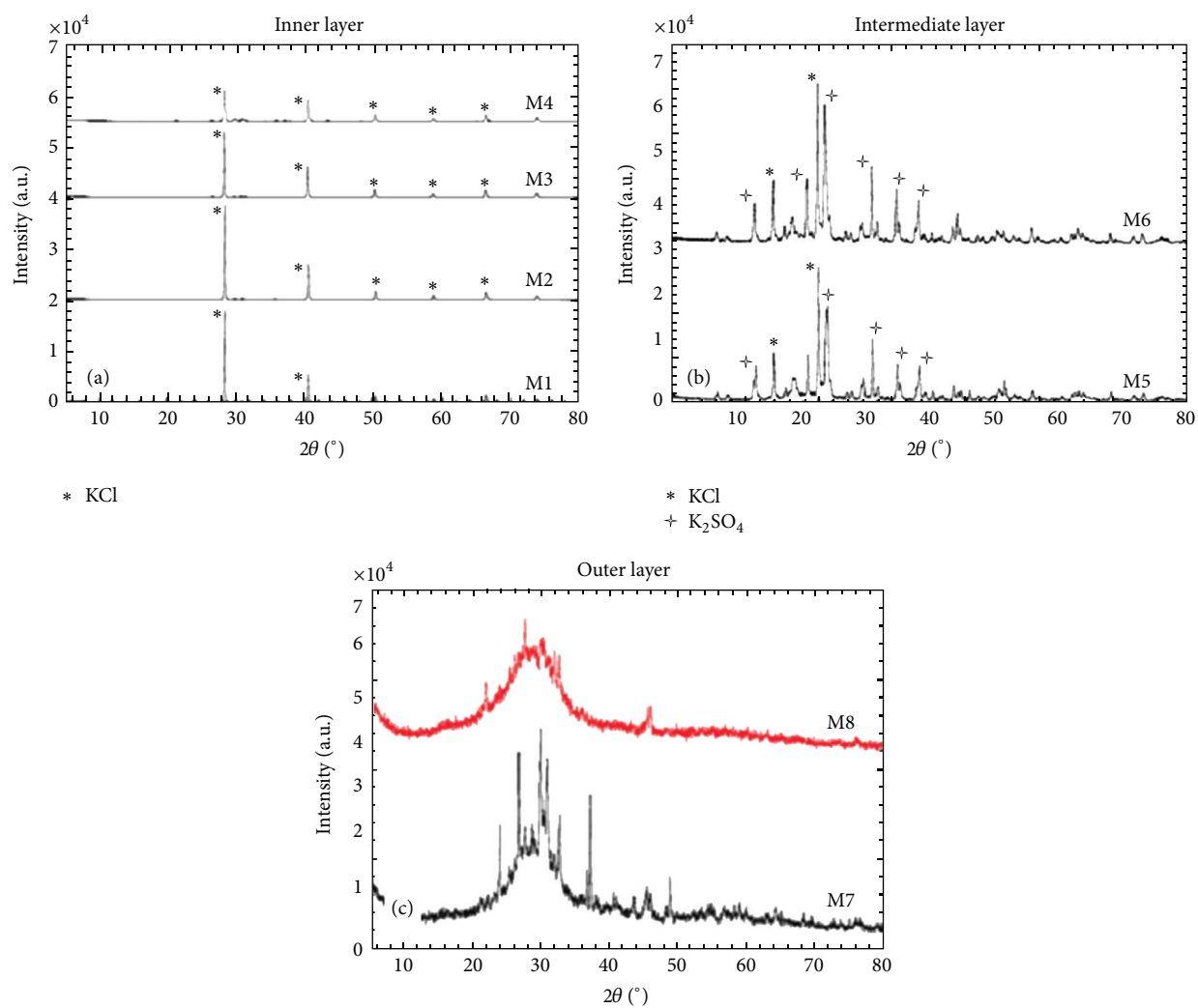


FIGURE 3: Diffractograms from the three layers. In the inner layer the peaks corresponds to the KCl; in the intermediate layer we can appreciate some peaks which correspond to  $K_2SO_4$  and in the outer the peaks indicate silicates.

the silicates composition increases. This fact agrees with similar studies carrying on oil-palm empty fruit bunch (biomass similar to straw related to content in Cl and K), where deposits were a thin inner white layer of KCl that condensate covering the entire probe surface and an outer grey layer consisting of KCl and Si-rich particles [3].

The outer layer is quite dense, which indicates that the layer has been molten. It is a compound of two phases (Figure 3(c)).

**3.3. Studies of the Oxides.** No peaks that can be associated with FeO(s), Cr<sub>2</sub>O<sub>3</sub>(s) nor to NiO(s) exist. The information on the diffraction of the phases has been obtained starting from the JCSP records (Figure 4).

The largest oxide is Fe<sub>2</sub>O<sub>3</sub>(s) and in smaller quantities Fe<sub>3</sub>O<sub>4</sub>(s). No peaks that can be associated with FeO(s) exist, Cr<sub>2</sub>O<sub>3</sub>(s) nor to NiO(s). Finally, the characteristic peaks of KCl(s) are observed.

**3.4. Studies of the Temperature.** Regarding the temperatures measured in superheaters 3 and 4, the great difference of temperatures is worth highlighting according to the localization of the thermopar. In any case, the temperatures (435–515°C) are lower than that expected, except for the thermopar number 12 (540–545°C).

## 4. Results Analysis

The results of the analysis of the corrosion of the superheaters tubes showed that the mechanism of more probable corrosion is that of active oxidation, which agrees with the literature.

As a final summary of the thermodynamic calculations carried out, one can affirm that of the three studied factors, Cl<sub>2</sub>(g) is the one that most favors the formation of solid and gaseous compounds with chlore. After accelerated oxidation is initiated by the presence of potassium, the presence of chloride is essential for it to continue [1, 27]. Chlorine is a small molecule which is likely to be able to diffuse through a deposit layer, rendering the protective oxide layer on the tube surface ineffective [6]. A higher chlorine concentration in the feed would result in higher tendency of deposition [28].

The quantity of KCl(s) has remained constant under all the conditions, from which it is deduced that it has not reacted with any element [29].

The most stable iron oxide of the plant has been Fe<sub>2</sub>O<sub>3</sub> and Fe<sub>3</sub>O<sub>4</sub>. However, regarding the mechanism of active oxidation, the rate of corrosion has been observed to be low for stainless steel AISI 347 CG (17). Also, hot corrosion is not observed because the salts do not melt at these low temperatures (450–500°C). On the other hand, it is necessary to bear in mind the metallurgists factors since the martensitic steel X20CrMoV suffered a high speed of corrosion [16] and was changed at 15.000 h while the rest of austenitic steels have been a good behaviour.

Another consideration is that excess alkali of biomass-based fuels may derive to KOH (ads.). Presence of KOH (ads.) on the heat transfer surfaces may be an important factor in the corrosion mechanisms in biomass-fired boilers [30].

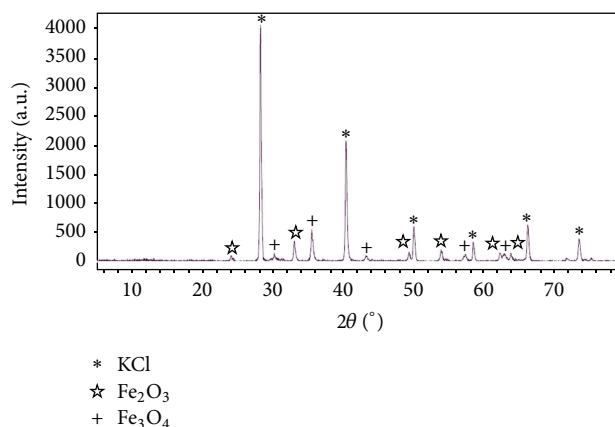


FIGURE 4: Diffractogram of the oxide formed on steel AISI 347 CG after 15,000 hours of testing in the superheater 3.

## 5. Conclusions

Cl<sub>2</sub>(g) is the main factor that favors the mechanism of active corrosion. The deposits formed on the superheaters tubes are formed by three layers of different chemical composition. The nearest to the tubes is mainly a compound of KCl(s) and it has a melting point of coalition of 575°C.


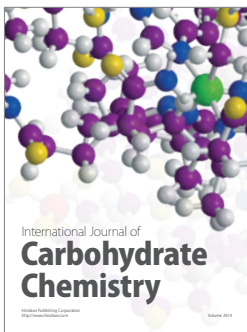
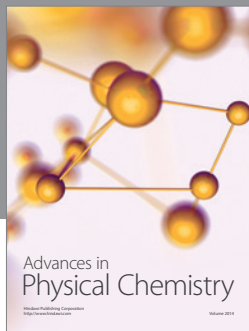
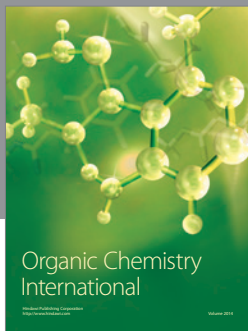
At current work temperatures of the plant the presence of KCl(s) on the tubes is not dangerous from the point of view of the corrosion.

## References

- [1] J. Lehmusto, D. Lindberg, P. Yrjas, B. Skrifvars, and M. Hupa, "Thermogravimetric studies of high temperature reactions between potassium salts and chromium," *Corrosion Science*, vol. 59, pp. 55–62, 2012.
- [2] W. Luo, Z. Liu, Y. Wang, and R. Yang, "High temperature corrosion behaviors of the superheater materials," *Procedia Engineering*, vol. 36, pp. 212–610, 2012.
- [3] T. Madhiyanon, P. Sathitruangsak, S. Sungworagarn, S. Pipatmanomai, and S. Tia, "A pilot-scale investigation of ash and deposition formation during oil-palm empty-fruit-bunch (EFB) combustion," *Fuel Processing Technology*, vol. 96, pp. 250–264, 2012.
- [4] M. S. Bashir, P. A. Jensen, F. Frandsen et al., "Ash transformation and deposit build-up during biomass suspension and grate firing: full-scale experimental studies," *Fuel Processing Technology*, vol. 97, pp. 93–106, 2012.
- [5] A. H. M. Khodier, T. Hussain, N. J. Simms, J. E. Oakey, and P. J. Kilgallon, "Deposit formation and emissions from co-firing miscanthus with Daw Mill coal: pilot plant experiments," *Fuel*, vol. 101, pp. 53–61, 2012.
- [6] J. Sandberg, C. Karlsson, and R. B. Fdhila, "A 7 year long measurement period investigating the correlation of corrosion, deposit and fuel in a biomass fired circulated fluidized bed boiler," *Applied Energy*, vol. 88, no. 1, pp. 99–110, 2011.
- [7] D. Nordgren, H. Hedman, N. Padban, D. Boström, and M. Öhman, "Ash transformations in pulverised fuel co-combustion of straw and woody biomass," *Fuel Processing Technology*, vol. 105, pp. 52–58, 2013.

- [8] M. Aho, T. Envall, and J. Kauppinen, "Corrosivity of flue gases during co-firing Chinese biomass with coal at fluidised bed conditions," *Fuel Processing Technology*, vol. 105, pp. 82–88, 2013.
- [9] S. Enestam, D. Bankiewicz, J. Tuiremo, K. Mäkelä, and M. Hupa, "Are NaCl and KCl equally corrosive on superheater materials of steam boilers?" *Fuel*, vol. 104, pp. 294–306, 2013.
- [10] O. Larsen and N. Henriksen, in *Proceedings of the International Conference on Power Plant Technology*, Kolding, Denmark, September 1996.
- [11] N. Henriksen, in *Proceedings of the VGB Conference Corrosion and Corrosion Protection in Power Plants*, Essen, Germany, November 1995.
- [12] F. J. Frandsen, H. P. Niesen, and P. A. Jensen, in *Proceedings of the Impact of Mineral Impurities in Solid Fuel Combustion*, Kona, Hawaii, USA, November 1997.
- [13] M. Montgomery and A. Karlson, *Materials and Corrosion*, vol. 50, pp. 579–584, 1999.
- [14] M. Montgomery, F. Frandsen, A. Karlson, and P. A. Jensen, United Engineering Foundations, New York, NY, USA, EPRI, 2001.
- [15] F. J. Frandsen, H. P. Niesen, and P. A. Jensen, *Proceedings of the CORROSION/2002 Research Topical Symposium*, Paper no. 02379, NACE International, Denver, Colo, USA, 2002.
- [16] C. Berlanga-Labari and J. Fernández-Carrasquilla, "Study of the oxidation to high temperature of eight alloys in atmospheres of combustion of biomass," *Revista de Metalurgia*, vol. 44, no. 4, pp. 343–354, 2008.
- [17] H. Kassman, M. Broström, M. Berg, and L. E. Åmand, "Measures to reduce chlorine in deposits: application in a large-scale circulating fluidised bed boiler firing biomass," *Fuel*, vol. 90, no. 4, pp. 1325–1334, 2011.
- [18] H. Kassman, J. Pettersson, B. Steenari, and L. Åmand, "Two strategies to reduce gaseous KCl and chlorine in deposits during biomass combustion— injection of ammonium sulphate and co-combustion with peat," *Fuel Processing Technology*, vol. 105, pp. 170–180, 2013.
- [19] L. Wang, J. E. Hustad, Ø. Skreiberg, G. Skjevraak, and M. Grønli, "A critical review on additives to reduce ash related operation problems in biomass combustion applications," *Energy Procedia*, vol. 20, pp. 20–29, 2012.
- [20] J. Silvennoinen and M. Hedman, "Co-firing of agricultural fuels in a full-scale fluidized bed boiler," *Fuel Processing Technology*, vol. 105, pp. 11–19, 2013.
- [21] M. Aho, P. Vainikka, R. Taipale, and P. Yrjas, "Effective new chemicals to prevent corrosion due to chlorine in power plant superheaters," *Fuel*, vol. 87, no. 6, pp. 647–654, 2008.
- [22] R. Weber, M. Mancini, N. Schaffel-Mancini, and T. Kupka, "On predicting the ash behaviour using Computational Fluid Dynamics," *Fuel Processing Technology*, vol. 105, pp. 113–128, 2013.
- [23] M. Becidan, L. Sørum, F. Frandsen, and A. J. Pedersen, "Corrosion in waste-fired boilers: a thermodynamic study," *Fuel*, vol. 88, no. 4, pp. 595–604, 2009.
- [24] M. Becidan and L. Sørum, "Consequences of unwanted local reducing conditions in biomass-fired boilers on chemistry and operation: a thermodynamic evaluation," *Energy and Fuels*, vol. 24, no. 3, pp. 1559–1564, 2010.
- [25] D. A. Shores and B. P. Mohanty, "Role of chlorides in hot corrosion of a cast Fe-Cr-Ni alloy, part II: thermochemical model studies," *Corrosion Science*, vol. 46, no. 12, pp. 2909–2924, 2004.
- [26] A. R. Outokumpu, *HSC Chemistry for Windows, Version 5*, Outokumpu Research, Espoo, Finland.
- [27] J. Lehmusto, B. Skrifvars, P. Yrjas, and M. Hupa, "Comparison of potassium chloride and potassium carbonate with respect to their tendency to cause high temperature corrosion of stainless 304L steel," *Fuel Processing Technology*, vol. 105, pp. 98–105, 2013.
- [28] Y. Shao, C. Xu, J. Zhu et al., "Ash and chlorine deposition during co-combustion of lignite and a chlorine-rich Canadian peat in a fluidized bed—effects of blending ratio, moisture content and sulfur addition," *Fuel*, vol. 95, pp. 25–34, 2012.
- [29] A. U. Syed, N. J. Simms, and J. E. Oakey, "Fireside corrosion of superheaters: effects of air and oxy-firing of coal and biomass," *Fuel*, vol. 101, pp. 62–73, 2012.
- [30] T. Blomberg, "Correlation of the corrosion rates of steels in a straw fired boiler with the thermodynamically predicted trend of KOH(g) in the flue gases," *Biomass and Bioenergy*, vol. 39, pp. 489–493, 2012.





**Hindawi**

Submit your manuscripts at  
<http://www.hindawi.com>

